Lagrangian Z-vector approach to Bethe–Salpeter analytic gradients: Assessing approximations

José D J Villalobos-Castro, Iryna Knysh, Denis Jacquemin, Ivan Duchemin, Xavier Blase

Lagrangian Z-vector Approach to Bethe-Salpeter Analytic Gradients: Assessing Approximations

José D.J. Villalobos-Castro,[1] Iryna Knysh,[2] Denis Jacquemin,[2,3] Ivan Duchemin,[4] and Xavier Blase[1]

[1)] *Univ. Grenoble Alpes, CNRS, Institut Néel, F-38042 Grenoble, France*

[2)] *Nantes Université, CNRS, CEISAM UMR 6230, F-44000 Nantes, France*

[3)] *Institut Universitaire de France (IUF), F-75005 Paris, France*

[4)] *Univ. Grenoble Alpes, CEA, IRIG-MEM-L_Sim, 38054 Grenoble, France*

We present an implementation of excited-state analytic gradients within the Bethe-Salpeter equation formalism using an adapted Lagrangian Z-vector approach with a cost independent of the number of perturbations. We focus on excited-state electronic dipole moments associated with the derivatives of the excited-state energy with respect to an electric field. In this framework, we assess the accuracy of neglecting the screened Coulomb potential derivatives, a common approximation in the Bethe-Salpeter community, as well as the impact of replacing the *GW* quasiparticle gradients by their Kohn-Sham analogs. The *pros* and *cons* of these approaches are benchmarked using both a set of small molecules for which very accurate reference data are available, and the challenging case of increasingly-extended push-pull oligomer chains. The resulting approximate Bethe-Salpeter analytic gradients are shown to compare well with the most accurate TD-DFT data, curing in particular most of the pathological cases encountered with TD-DFT when a non-optimal exchange-correlation functional is used.

I. INTRODUCTION

The wealth of phenomena associated with both photophysical and photochemical processes, characterized by strong electronic and structural reorganizations away from the ground-state (GS), offers a strong motivation for developing theoretical tools allowing to study the properties of condensed matter systems in their excited states (ES). Beyond the standard determination of ES energies, their gradients with respect to nuclear positions provide the forces needed to follow the structural reorganisation associated with, e.g., a photoinduced chemical reaction. Likewise, another gradient, the derivative of the ES total energy with respect to an applied electric field, gives access to the ES electronic dipole moments, a key signature of the electronic rearrangement upon excitation. Excited-state dipole moments are important properties from both an experimental point of view, as they provide an hint at the charge-transfer character of the considered state, and from a theoretical perspective, since they are likely the simplest property that can be directly related to the ES density. The experimental characterization of ES dipoles through Stark effect measurements or solvatofluorochromism is a difficult task,[1,2] leaving theory as an important source of information on the ES charge distribution. Indeed, Stark measurements use the deformation of the vibronic bands under an external electric field to determine the ES dipole, an approach only applicable for small gas phase molecules, whereas the measurements of the evolution of the fluorescence peak position in solvents of different polarity provide estimates of the ES dipole of (large) solvated molecules, but generally under a simplified physical model. In other words, both experimental techniques produce data coming with significant incertitudes.

Besides numerical gradients relying on finite-field (or finite-difference) techniques, analytic gradients of ES energies were introduced in quantum chemistry as an extension to Coupled-Perturbed Hartree-Fock (CPHF) or Kohn-Sham (CPKS)[3–5] calculations of the perturbed molecular orbitals. Such direct techniques require solving the CPHF/CPKS equation as many times as there are perturbations, namely $3N_{\text{at}}$ times in the case of nuclear gradients in a molecule containing N_{at} atoms. It was early recognized, on the basis of the Handy-Schaeffer Z-vector technique,[6] that in fact most of the needed operations could be factorized in such a way that all ES gradients can be obtained for the cost of a single CPHF/CPKS calculation. The Z-vector equation formalism was further simplified using an elegant Lagrangian formalism allowing to bypass the explicit calculation of the molecular orbitals gradients.[7,8] Such a Lagrangian Z-vector approach is now implemented in many codes for calculating ES gradients within time-dependent density-

functional theory (TD-DFT),[9] including extensions to polarizable environments,[10,11] and as well as many-body wavefunction approaches such as coupled-cluster (CC) techniques.[12–14]

In recent years, the Bethe-Salpeter equation (BSE)[15–20] formalism has generated much interest to study the optical properties of molecular organic systems with several benchmarks performed on diverse molecular families,[21–28] allowing comparison with both wavefunction theories and TD-DFT approaches. The Bethe-Salpeter formalism to neutral electronic excitations, offering the same cost as TD-DFT calculations, was in particular shown to offer an accuracy equivalent to TD-DFT calculations performed with optimised (tuned) exchange-correlation functionals (XCFs), notably addressing the difficulties associated with charge-transfer,[23,29–35] Rydberg[23] and cyanine[36] ES. Extension to dynamical kernels,[37–41] GS total energies,[42–44] core-level spectroscopies,[45–47] are examples of developments extending the applicability of BSE calculations to molecular systems. Finally, and beyond the study of isolated gas phase molecular systems, standard techniques to deal with systems embedded in a polarizable environment have been adapted to the BSE formalism, including both continuum[48,49] and discrete[50,51] models of polarizable environments, together with fragments or subsystem-based approaches allowing to treat large systems.[52–54] However, a strong limitation with the BSE approach is the lack of efficient formalisms to calculate ES energy gradients.

In a pioneering study, the structural relaxation of the lowest ES of two small molecules (CO and NH_3) was studied with the BSE formalism,[55] implementing a direct analytic formalism based on Density Functional Perturbation Theory (DFPT)[56] with a cost proportional to the number of perturbations. In that study, analytic gradients were implemented relying on two simplifications: *i*) the neglect of the gradient of the screened Coulomb potential W, an historical approximation in the BSE community, and *ii*) the replacement of the *GW* quasiparticle energy gradients by their KS analogs. These two approximations, that dramatically reduce the cost of calculating BSE gradients, were shown to be accurate for these two model systems. Later, finite-field techniques were used to study the BSE ES structural relaxation for carbon monoxide, acetone, acrolein, and methylenecyclopropene.[57] Further, the challenging evolution and crossing of ES potential energy surfaces upon twist angle in retinal,[58] dimethylaminobenzonitrile[59] and N-phyenylpyrrole molecules[60] were explored, suggesting accurate BSE nuclear gradients in more complex organic systems. Finally, the ES dipole moments of increasingly long pus-pull chains were calculated at the finite-field BSE level with comparison to CC calculations,[61] a work demonstrating the accuracy of BSE ES dipoles for a challenging case.

In the present study, we explore a simplified BSE analytic gradients approach within a Z-vector Lagrangian formalism focusing on ES dipole moments. In the standard Z-vector equation, that we write symbolically $(A+B)Z = R$, we find that the $(A+B)$ matrix is rigorously the same as in TD-DFT calculations, provided that the preceding *GW* calculations are performed at a non-self-consistent or partially self-consistent level preserving the one-body $\{\phi_n^{KS}\}$ input KS molecular orbitals used to calculate the *GW* operator and BSE electron-hole Hamiltonian. As such, the two implemented approximations, namely *i*) neglecting the gradients of the screened Coulomb potential, and *ii*) identifying the *GW* quasiparticle gradients to their KS analogs, only modify the right-hand-side R vector. We illustrate the merits and limitations of these two simplifications on a set of small molecules for which high-level reference quantum chemistry calculations are available,[62,63] as well as on the above-mentioned increasingly long push-pull oligomers.[61,64] We show in particular that the use in the R-vector of the screened-Coulomb potential W, mediating non-local electron-hole interactions, can significantly correct the pathological gradients obtained with TD-DFT calculations based on XC kernels containing an insufficient amount of exact exchange. Further, simplification *i*) is shown to be an excellent approximation, while approximation *ii*) is found to be much less innocent, unless an optimally-tuned XC functional is used at the input Kohn-Sham level. Overall, this simplified BSE Z-vector formalism is shown to provide results *on par* with the best (tuned) TD-DFT calculations.

II. THEORY

We briefly review the Green's function many-body perturbation *GW*[65–68] and Bethe-Salpeter equation (BSE) formalisms,[15–20] focusing on the aspects relevant to the subsequent ES gradients calculations. Extensive reviews on the *GW* and BSE methods can be found in the literature.[15,69–75] The basic equations associated with the Z-vector Lagrangian formulation of ES gradients[8,11] are then reviewed, focusing on the modifications and approximations underlying the use of the *GW* quasiparticle energies and BSE excitonic Hamiltonian in place of their Kohn-Sham DFT and TD-DFT analogs.

A. The *GW* and Bethe-Salpeter equation formalisms

Stemming from many-body perturbation theory, the *GW* approximation to the exchange-correlation potential, labeled a self-energy, reads:

$$\Sigma^{GW}(\mathbf{r},\mathbf{r}';E) = \frac{i}{2\pi}\int d\omega\, e^{i\omega\eta} G(\mathbf{r},\mathbf{r}';E+\omega)W(\mathbf{r},\mathbf{r}';\omega) \tag{1}$$

where η is a positive infinitesimal, G the one-body time-ordered Green's function, and W the dynamically screened Coulomb potential. Such a Green's function formalism allows calculating electronic energy levels that can be formally related to the output of a photoemission experiment, namely to proper ionization potentials and electronic affinities. The *GW* self-energy is not exact but stems from a lowest-order perturbation approach in terms of the random-phase-approximation (RPA) screened Coulomb potential W. Further, in practice, the needed Green's function G is taken to be that associated with input Kohn-Sham one-body eigenstates and energy levels:

$$G(\mathbf{r},\mathbf{r}';\omega) = \sum_n \frac{\phi_n^{\rm KS}(\mathbf{r})[\phi_n^{\rm KS}(\mathbf{r}')]^*}{\omega-\varepsilon_n^{\rm KS}+i\eta\times{\rm sign}(\varepsilon_n^{\rm KS}-\mu)} \tag{2}$$

with μ the chemical potential. In the following, the wording KS eigenstates will include molecular orbitals (MOs) and related energy levels stemming from DFT, Hartree-Fock or hybrid XCF calculations. The dynamically screened Coulomb potential stems from the construction of the Kohn-Sham independent-electron susceptibility χ_0 within the (direct) RPA, namely:

$$\begin{aligned} W(\mathbf{r},\mathbf{r}';\omega) &= V(\mathbf{r},\mathbf{r}') \\ &\quad + \int d\mathbf{r}_1 d\mathbf{r}_2\, V(\mathbf{r},\mathbf{r}_1)\chi_0(\mathbf{r}_1,\mathbf{r}_2;\omega)W(\mathbf{r}_2,\mathbf{r}';\omega) \end{aligned} \tag{3}$$

$$\chi_0(\mathbf{r},\mathbf{r}';\omega) = \sum_{ia} \frac{[\phi_a^{\rm KS}(\mathbf{r})]^*\phi_i^{\rm KS}(\mathbf{r})[\phi_i^{\rm KS}(\mathbf{r}')]^*\phi_a^{\rm KS}(\mathbf{r}')}{\omega-(\varepsilon_a^{\rm KS}-\varepsilon_i^{\rm KS})+i\eta} + c.c. \tag{4}$$

adopting here and below quantum chemistry notations with (i,j) pointing to occupied orbitals, (a,b) to virtual (unoccupied) ones, and (m,n,p,q,r,s) to any orbital. In practice, the most common *GW* schemes assume that the Hamiltonian, or Fock operator, $\hat{F}^{GW}$ built with the *GW* self-energy, is diagonal in the Kohn-Sham molecular orbital basis, so that the input KS energy levels can be corrected as follows:

$$\varepsilon_n^{GW} = \varepsilon_n^{\rm KS} + \langle\phi_n^{\rm KS}|\Sigma^{GW}(\mathbf{r},\mathbf{r}';\varepsilon_n^{GW}) - V_{XC}^{\rm KS}|\phi_n^{\rm KS}\rangle \tag{5}$$

where $V_{XC}^{\rm KS}$ is the Kohn-Sham exchange-correlation (XC) mean-field potential. The dynamical self-energy Σ^{GW} has to be calculated at the ε_n^{GW} targeted energy. Such a scheme, where input

Kohn-Sham eigenstates are used to build the *GW* self-energy operator is called the single-shot or G_0W_0 approach. From the corrected $\{\varepsilon_n^{GW}\}$ electronic energy levels, labeled quasiparticle energies, an updated G and W can be calculated, while keeping input Kohn-Sham molecular orbitals frozen. This is the so-called partially self-consistent approach with self-consistent update of the energy levels, an approach labeled *evGW*. Such an approach has been shown to offer an excellent accuracy at reduced cost as compared to fully self-consistent approaches where one-body molecular orbitals are also updated.[76]

Concerning now the Bethe-Salpeter equation (BSE) formalism, the relation between the charge density and the diagonal of the Green's function: $n(\mathbf{r},t) = -iG(\mathbf{r}t,\mathbf{r}t^+)$, with $t^+ = (t+\eta)$ in a time representation, allows to generalize the standard TD-DFT electronic susceptibility by introducing a four-point susceptibility as the derivative of the Green's function by a non-local perturbation: $L(1,2,3,4) = \partial G(1,2)/\partial U(3,4)$ with *e.g.* $1 = (\mathbf{r}_1 t_1)$ in space-time notations. The resulting BSE excitation energies $\{\Omega_\lambda\}$ and two-body (electron-hole) eigenstates $\psi_\lambda(\mathbf{r}_e,\mathbf{r}_h)$:

$$\psi_\lambda^{\mathrm{BSE}}(\mathbf{r}_e,\mathbf{r}_h) = \sum_{ia}\left[X_{ia,\lambda}^{\mathrm{BSE}}\phi_a(\mathbf{r}_e)\phi_i(\mathbf{r}_h) + Y_{ia,\lambda}^{\mathrm{BSE}}\phi_a(\mathbf{r}_h)\phi_i(\mathbf{r}_e)\right] \tag{6}$$

with $(\mathbf{r}_e,\mathbf{r}_h)$ electron and hole positions and where (λ) indexes the excitations, can be obtained by solving the following eigenvalue system in the product (occupied)$\times$(virtual) transition space:

$$\left(\Lambda^{\mathrm{BSE}} - \Omega\Delta\right)\begin{pmatrix} X \\ Y \end{pmatrix} = 0 \tag{7}$$

with Λ^{BSE} the BSE Hamiltonian and Δ the relevant metric to deal with the normalization of excitation/de-excitation processes:

$$\Lambda^{\mathrm{BSE}} = \begin{pmatrix} A^{\mathrm{BSE}} & B^{\mathrm{BSE}} \\ B^{\mathrm{BSE}} & A^{\mathrm{BSE}} \end{pmatrix} \quad \Delta = \begin{pmatrix} 1 & 0 \\ 0 & -1 \end{pmatrix} \tag{8}$$

For closed-shell systems:

$$A_{ia,jb}^{\mathrm{BSE}} = (\varepsilon_a^{GW} - \varepsilon_i^{GW})\delta_{ab}\delta_{ij} + \kappa(ia|jb) - W_{ij,ab} \tag{9a}$$

$$B_{ia,jb}^{\mathrm{BSE}} = \kappa(ia|bj) - W_{ib,aj} \tag{9b}$$

with $\kappa = 2$ and 0 respectively for singlet and triplet excitations adopting the following Coulomb integrals notations :

$$(ia|jb) = \int d\mathbf{r}d\mathbf{r}'\ \phi_i(\mathbf{r})\phi_a(\mathbf{r})V(\mathbf{r},\mathbf{r}')\phi_j(\mathbf{r}')\phi_b(\mathbf{r}') \tag{10}$$

$$W_{ia,jb} = \int d\mathbf{r}d\mathbf{r}'\ \phi_i(\mathbf{r})\phi_a(\mathbf{r})W(\mathbf{r},\mathbf{r}';0)\phi_j(\mathbf{r}')\phi_b(\mathbf{r}') \tag{11}$$

We use here real-valued MOs for finite size systems without applied magnetic field. In the standard BSE formalism, the screened Coulomb potential is taken to be static, an approximation equivalent to the adiabatic formulation of the TD-DFT kernel.

For what follows, it is worthwhile noticing that the BSE matrix formulation is formally close to time-dependent Hartree-Fock (TD-HF) upon replacing the *GW* quasiparticle energies by the Hartree-Fock ones and the screened Coulomb potential by its bare analog. Such a formal proximity allows to set up intermediate validation steps through the implementation of TD-HF analytic gradients within the Lagrangian *Z*-vector formalism. This is described in the Supplementary Material (SM) Table S1.

We further note that the BSE excited-state unrelaxed electron density, namely the probability of finding an electron in $\mathbf{r}_e$ averaging over the hole degrees of freedom, and the related hole density, reads:

$$\rho_{e/h}(\mathbf{r}_{e/h}) = \int d\mathbf{r}_{h/e} \, |\psi_\lambda^{\mathrm{BSE}}(\mathbf{r}_e, \mathbf{r}_h)|^2 \tag{12}$$

leading through the orthogonality of the molecular orbitals to:

$$\rho_e(\mathbf{r}_e) = \sum_{iab} X_{ia}X_{ib}\phi_a(\mathbf{r}_e)\phi_b(\mathbf{r}_e) - \sum_{ija} Y_{ia}Y_{ja}\phi_i(\mathbf{r}_e)\phi_j(\mathbf{r}_e) \tag{13}$$

$$\rho_h(\mathbf{r}_h) = -\sum_{iab} Y_{ia}Y_{ib}\phi_a(\mathbf{r}_h)\phi_b(\mathbf{r}_h) + \sum_{ija} X_{ia}X_{ja}\phi_i(\mathbf{r}_h)\phi_j(\mathbf{r}_h) \tag{14}$$

with special care to the (-1) factor in the Y-coefficients multiplication associated with the normalization of the BSE eigenstates. The unrelaxed electron density variation from the ground-state to the excited-state can be obtained as the difference $[\rho_e(\mathbf{r}) - \rho_h(\mathbf{r})]$ leading in compact notations to :

$$\Delta\rho(\mathbf{r}) \overset{\text{unrlxd}}{=} \sum_{pq} T_{pq}\phi_p(\mathbf{r})\phi_q(\mathbf{r}) \tag{15}$$

$$T_{ij} = -\sum_a \left(X_{ia}X_{ja} + Y_{ia}Y_{ja}\right) \tag{16}$$

$$T_{ab} = \sum_i \left(X_{ia}X_{ib} + Y_{ia}Y_{ib}\right) \tag{17}$$

a formulation identical to the standard TD-DFT definition with $T_{ia} = T_{ai} = 0$. The relaxation of the molecular orbitals upon excitation yields a correction to the unrelaxed T difference density matrix. Such a correction is precisely the *Z*-vector.

B. Lagrangian Z-vector formalism

To briefly introduce the interest of the Lagrangian Z-vector approach, let us consider a perturbation labeled (ζ) and the gradient of an excitation energy Ω_λ with respect to this perturbation:

$$\Omega_\lambda^\zeta = \langle X_\lambda, Y_\lambda | \Lambda^\zeta | X_\lambda Y_\lambda \rangle \tag{18}$$

where the superscript (ζ) indicates a derivative by the perturbation. The matrix Λ could be the TD-DFT, TD-HF, or BSE one. The derivative of the $\{X_{ia,\lambda}\}$ coefficients vanish by orthonormalization of the Λ-matrix eigenstates (Hellmann-Feynman theorem). In a standard approach, the expression of the Λ-matrix elements as a function of the KS eigenstates and associated KS or *GW* energies, leads to performing standard perturbation theory to obtain the gradients $\{\phi_{i/a}^\zeta\}$ and $\{\varepsilon_{i/a}^\zeta\}$. Such MOs eigenstates derivatives can be obtained within the framework of DFPT,[56,77,78] as done by Ismail-Beigi and Louie for the calculation of the BSE ionic gradients of CO and NH_3,[55] or within the CPHF/KS approach.[3–5] DFPT, within its modern Green's function formulation and its adaptation to periodic systems, is more common in the physicist community, while CPKS is the method typically implemented in quantum chemistry codes.

Independently of the approach used to perform perturbation theory, such calculations must be performed for *each external perturbation*. This is the great advantage of the Lagrangian formalism that requires only one system of that kind to be solved for all perturbations, the cost of the remaining perturbation-dependent operations to be performed being marginal. Following Furche and Ahlrichs,[8] based on an idea by Helgaker and Jørgensen,[7] we define a functional:

$$L[X,Y,\Omega,C,Z,W,\zeta] = \underline{G}[X,Y,\Omega] + \sum_{ia} Z_{ia} F_{ia} - \sum_{rs,r\leq s} W_{rs}^L (S_{rs} - \delta_{rs}) \tag{19}$$

where $F_{ia} = \langle i|\hat{F}|a\rangle$ and $S_{rs} = \langle r|s\rangle$ are the Hamiltonian and overlap matrix elements between MOs. The $\{Z_{ia}\}$ and $\{W_{rs}^L\}$ are Lagrange multipliers enforcing that $F_{ia} = 0$ and $S_{rs} = \delta_{rs}$ *at the global minimum* of L. The functional $\underline{G}[X,Y,\Omega]$ is associated with the (vertical) excitation energies:

$$\underline{G}[X,Y,\Omega] = \langle X,Y|\Lambda|X,Y\rangle - \Omega\left(\langle X,Y|\Delta|X,Y\rangle - 1\right) \tag{20}$$

where the operator Λ could be associated with TD-DFT, TD-HF, or BSE. To prevent confusion with the Green's function G, we chose to underline the G-functional generally introduced. Similarly, we label the Lagrange parameters W_{rs}^L - with the superscript L for Lagrange - to prevent confusion with the screened Coulomb potential W. We also include the perturbation ζ in the list

of variables since now the L functional bears an explicit functional of the perturbation through the Hamiltonian $\hat{F}$, with, *e.g.*, in the case of switching a uniform E-field along the $\hat{x}$-direction:

$$F_{ia} \Longrightarrow F_{ia} - eE\langle i|x|a\rangle \tag{21}$$

The "C" variables in the definition of L point to the molecular orbital coefficients in the chosen basis:

$$|n\rangle = \sum_{\mu} C_{n\mu}|\chi_{\mu}\rangle \tag{22}$$

where the index (μ) runs over the atomic basis $\{\chi_{\mu}\}$. The key point now is that the minimization of L with respect to the perturbation (ζ) leads to:

$$\Omega^{\zeta} = \langle X,Y|\underline{G}^{(\zeta)}|X,Y\rangle - \sum_{ia} Z_{ia}F_{ia}^{(\zeta)} - \sum_{rs,r\leq s} W_{rs}^{L}S_{rs}^{(\zeta)} \tag{23}$$

with the notation that $\underline{G}^{(\zeta)}, F_{ia}^{(\zeta)}, S_{rs}^{(\zeta)}$ are derivatives taken at the frozen (X,Y,Ω,C,Z) values that minimize L. This is the great advantage of the present Lagrangian formalism that the derivative of $\underline{G}$ can be taken at constant $\{C_{\mu n}\}$ coefficients, without the need to perform DFPT or CPKS calculations for each perturbation. The price to pay is the evaluation of the $\{Z_{ia}, W_{rs}^{L}\}$ Lagrange parameters. Since such parameters are obtained by the minimization of L with respect to the $\{C_{\mu n}\}$ coefficients *at frozen* ζ, namely in the absence of the perturbation, these coefficients are perturbation-independent and can be obtained at the cost of a single CPKS-like resolution.

While the previous equations originate directly from the seminal TD-DFT treatment,[8] we now discuss the specificities introduced by the *GW* and BSE formalisms. As emphasized above, most *GW* and BSE calculations, even partially self-consistent *evGW* calculations, are performed without updating the input KS MOs. Only the electronic energy levels are updated by the *GW* correction. Consequently, the $Z_{ia}F_{ia}$ constraint appearing in the L functional, enforcing that the MOs are the proper solution of the $\hat{F}$ Hamiltonian at the global minimum of L, should be constructed with the $\hat{F}^{KS}$ KS Hamiltonian. Further, the overlap matrix S and the MO coefficients $\{C\}$ are the Kohn-Sham ones as well. As such:

$$L[X,Y,\Omega,C^{\mathrm{KS}},Z,W,\zeta] \overset{evGW}{=} \underline{G}^{\mathrm{BSE}}[X,Y,\Omega] + \sum_{ia} Z_{ia}F_{ia}^{\mathrm{KS}} - \sum_{rs,r\leq s} W_{rs}^{L}(S_{rs}^{\mathrm{KS}} - \delta_{rs}) \tag{24}$$

for standard BSE calculations relying on G_0W_0 and *evGW* calculations. As shown now, this really means that the left-hand-side operator acting on Z, in the Z-vector equation, is the one associated

with the KS formalism used to provide the MOs needed to build the *GW* operator. The difference between TD-DFT and BSE analytic Z-vector equations will only affect the right-hand-side R-vector as discussed below. The Z-vector equation stems from the minimisation of L with respect to the MO coefficients:

$$\frac{\partial L}{\partial C_{\mu p}} = 0 \tag{25}$$

where we have removed the KS superscript from the $\{C_{\mu p}\}$ coefficients, or in a restricted fashion:

$$\sum_{\mu} \frac{\partial L}{\partial C_{\mu p}} C_{\mu q} = 0 \tag{26}$$

with $(pq = ia)$ and $(pq = ai)$ that yields sufficient conditions to obtain the needed Z_{ia} factors. This can be rewritten as:

$$Q^{\mathrm{BSE}}_{pq} + \sum_{ia} Z_{ia} \sum_{\mu} \frac{\partial F^{\mathrm{KS}}_{ia}}{\partial C_{\mu p}} C_{\mu q} = \sum_{rs, r \leq s} W^{L}_{rs} \sum_{\mu} \frac{\partial S^{\mathrm{KS}}_{rs}}{\partial C_{\mu p}} C_{\mu q} \tag{27}$$

with

$$Q^{\mathrm{BSE}}_{pq} = \sum_{\mu} C_{\mu q} \frac{\partial G^{\mathrm{BSE}}}{\partial C_{\mu p}} \tag{28}$$

Straightforward derivation leads to :

$$\sum_{rs, r \leq s} W^{L}_{rs} \sum_{\mu} \frac{\partial S^{\mathrm{KS}}_{rs}}{\partial C_{\mu p}} C_{\mu q} = W^{L}_{pq}(1 + \delta_{pq}) \tag{29}$$

From the $Z_{ia} F^{\mathrm{KS}}_{ia}$ constraint built with the Kohn-Sham Hamiltonian, one obtains as in standard TD-DFT[8]:

$$\sum_{ia} Z_{ia} \sum_{\mu} \frac{\partial F^{\mathrm{KS}}_{ia}}{\partial C_{\mu p}} C_{\mu q} = \varepsilon^{\mathrm{KS}}_{q} Z_{pq} \times |f_q - f_p| + H^{+,KS}_{pq}[Z] \times \theta(\mu - \varepsilon^{\mathrm{KS}}_{p}) \tag{30}$$

with $(f_{q/p})$ occupation factors, μ the chemical potential, and the operators:

$$H^{+,\mathrm{KS}}_{ia}[Z] = \sum_{jb} H^{+,\mathrm{KS}}_{ia,jb} Z_{jb} \tag{31a}$$

$$H^{+,\mathrm{KS}}_{ia,jb} = 4(ia|jb) + 4 f^{\mathrm{XC}}_{ia,jb} - c_X[(ij|ab) + (ia|jb)] \tag{31b}$$

where f^{KS} is the DFT exchange-correlation kernel and c_X the amount of (global) exact exchange. We have adopted here the closed-shell expression with e.g. $j = 1 \rightarrow N/2$. With the Kohn-Sham

Hamiltonian only depending on occupied states, the $H^{+,KS}$ contribution stemming from the derivative $\langle i|[\partial \hat{F}^{\mathrm{KS}}/\partial C_{\mu p}]|a\rangle$ only occurs for (p) pointing to an occupied state. With $(pq = ia)$ and $(pq = ai)$ one obtains two equations:

$$Q_{ia}^{\mathrm{BSE}} + \varepsilon_a^{\mathrm{KS}} Z_{ia} + H_{ia}^{+,\mathrm{KS}}[Z] = W_{ia}^L \tag{32a}$$

$$Q_{ai}^{\mathrm{BSE}} + \varepsilon_i^{\mathrm{KS}} Z_{ia} = W_{ia}^L \tag{32b}$$

accounting for the imposed equalities $(Z_{ia} = Z_{ai})$ and $(W_{ia}^L = W_{ai}^L)$. The difference between Eqs. 32a and 32b yields:

$$(\varepsilon_a^{\mathrm{KS}} - \varepsilon_i^{\mathrm{KS}}) Z_{ia} + H^{+,\mathrm{KS}}[Z] = R_{ia}^{\mathrm{BSE}} \tag{33a}$$

$$R_{ia}^{\mathrm{BSE}} = -(Q_{ia}^{\mathrm{BSE}} - Q_{ai}^{\mathrm{BSE}}) \tag{33b}$$

As hinted above, the left-hand-side operator acting on the Z vector is identical to that used in the CPKS equation, or CPHF for $f^{\mathrm{XC}} = 0$ and $c_X = 1$. The present Z-vector equation, or the CPHF/CPKS problem, can be solved iteratively, involving (matrix$\times$vector) multiplications in transitions space, namely an $\mathscr{O}(N^4)$ computational effort. As emphasized above, a key feature is that the eigen-system from which the Z vector can be obtained is independent of whatever applied perturbation.

C. The Bethe-Salpeter Q^{BSE} vectors

We now wish to calculate the derivatives of $(\partial \underline{G}^{BSE}/\partial C_{\mu p})$ following eq. 28. Adapting an idea introduced in the case of TD-DFT,[8] we rewrite the diagonal part of the BSE functional composed of the *GW* quasiparticle energies using the transformation:

$$(\varepsilon_a^{\mathrm{GW}} - \varepsilon_i^{\mathrm{GW}})\delta_{ij}\delta_{ab} \Longrightarrow F_{ab}^{\mathrm{GW}}\delta_{ij} - F_{ij}^{\mathrm{GW}}\delta_{ab} \tag{34}$$

with F_{rs}^{GW} the *GW* Hamiltonian matrix elements in the Kohn-Sham basis. Such a transformation allows to make the MOs and related $\{C_{\mu p}\}$ coefficients explicit, and leads to the following expression:

$$\begin{aligned}\underline{G}^{\mathrm{BSE}}[X,Y,\Omega] = &\sum_{rs} F_{rs}^{\mathrm{GW}} T_{rs} - \Omega\left[\left(\sum_{ia}(X_{ia}^2 - Y_{ia}^2)\right) - 1\right] \\ &+ \sum_{ia,jb} K_{ia,jb}^{\mathrm{BSE}}\left(X_{ia}X_{jb} + Y_{ia}Y_{jb}\right) \\ &+ \sum_{ia,jb} K_{ia,bj}^{\mathrm{BSE}}\left(X_{ia}Y_{jb} + Y_{ia}X_{jb}\right)\end{aligned} \tag{35}$$

where the BSE kernel reads:

$$K^{\mathrm{BSE}}_{ia,jb} = 2(ia|jb) - W_{ij,ab}(\omega = 0) \tag{36a}$$

$$K^{\mathrm{BSE}}_{ia,bj} = 2(ia|bj) - W_{ib,aj}(\omega = 0) \tag{36b}$$

for singlet excitations as considered in this study. Here the (X,Y) and resulting T coefficients are the BSE ones for a given excitation. The derivatives have to be taken at constant (X,Y,Ω). This leads to evaluate the derivatives of the GW quasiparticle energies and BSE kernel matrix elements.

The BSE kernel written here above relies in particular on the neglect of the $(\partial W/\partial G)$ variation in the needed $(\partial GW/\partial G)$ variation of the GW self-energy. This is a central approximation in the large majority of BSE implementations. As such, and with W a functional $W[G]$ of the Green's function, any derivative of W by some external perturbation may consistently be neglected following the chain rule $(\partial W/\partial \zeta) = (\partial W/\partial G)\cdot(\partial G/\partial \zeta)$. In that approximation, the gradients of the $K_{ia,jb}$ matrix elements only stem from that of the molecular orbitals, leading e.g. to:

$$\sum_{\mu} C_{\mu q} \frac{\partial K^{\mathrm{BSE}}_{ia,jb}}{\partial C_{\mu p}} = \delta_{pi} K^{\mathrm{BSE}}_{qa,jb} + \delta_{pa} K^{\mathrm{BSE}}_{iq,jb} + \delta_{pj} K^{\mathrm{BSE}}_{ia,qb} + \delta_{pb} K^{\mathrm{BSE}}_{ia,jq} \tag{37}$$

Concerning now the derivative of the electronic energy levels through the F^{GW}_{rs} matrix elements, we obtain:

$$\sum_{\mu} C_{\mu q} \frac{F^{GW}_{rs}}{\partial C_{\mu p}} = \varepsilon^{GW}_{q}(\delta_{pr}\delta_{qs} + \delta_{ps}\delta_{qr}) + \sum_{\mu} C_{\mu q} \langle r| \frac{\partial \hat{F}^{GW}}{\partial C_{\mu p}} |s\rangle \tag{38}$$

With $(rs = ab/ij)$ and $(pq = ia/ai)$, the ε^{GW}_{q} disappears and the distinction between using GW or Kohn-Sham energy levels is irrelevant. Remains however the explicit derivation of the $\hat{F}^{GW}$ Hamiltonian that we can rewrite as:

$$\langle r| \frac{\partial \hat{F}^{GW}}{\partial C_{\mu p}} |s\rangle = \langle r| \frac{\partial \hat{F}^{\mathrm{KS}}}{\partial C_{\mu p}} |s\rangle + \langle r| \frac{\partial (\Sigma^{GW} - V^{\mathrm{DFT}}_{\mathrm{XC}})}{\partial C_{\mu p}} |s\rangle \tag{39}$$

In the case of a HF starting point, the difference $(\Sigma^{GW} - V^{\mathrm{DFT}}_{\mathrm{XC}})$ is just the correlation part of the GW operator. The derivation $\langle r|[\partial \Sigma^{GW}/\partial C_{\mu p}]|s\rangle$ can in principle be performed, even though involving off-diagonal GW matrix elements in the KS basis. This is at odds with the diagonal approximation on which the evGW scheme relies. The main approximation of the present study is thus to neglect the gradients of the $(\Sigma^{GW} - V^{\mathrm{DFT}}_{\mathrm{XC}})$ correction in the R_{ia} vector. Such an approximation will be explored here below by comparison with finite-field calculations.

At this stage, let us compare the present scheme to the calculations performed by Ismail-Beigi and Louie using direct DFPT calculations for each perturbation,[55] with the same approximation

consisting in equating the $\{\partial^\zeta \varepsilon_n^{GW}\}$ gradients with their $\{\partial^\zeta \varepsilon_n^{KS}\}$ LDA Kohn-Sham analogs in the case of the model CO and NH_3 molecules. Such an approximation was shown to be accurate, even though the LDA Kohn-Sham energy levels are known to differ by several electronvolts from the *GW* quasiparticle energies for small molecular systems. This hinges on the idea that even though the quasiparticle correction $(\varepsilon_n^{GW} - \varepsilon_n^{\mathrm{KS}})$ can be large, its gradient may be limited.

Overall, the gradients of the BSE kernel and of the diagonal KS $(\varepsilon_a - \varepsilon_i)$ energy differences allow building the Q and R vectors needed on the right-hand-side of the Z-vector equation, with:

$$\begin{aligned} R_{ia} = & -H_{ia}^{+,KS}[T] \\ & + 2\sum_j (K_{ji}^{BSE}[X] + K_{ij}^{BSE}[Y])X_{ja} + (K_{ji}^{BSE}[Y] + K_{ij}^{BSE}[X])Y_{ja} \\ & - 2\sum_b (K_{ab}^{BSE}[X] + K_{ba}^{BSE}[Y])X_{ib} + (K_{ab}^{BSE}[Y] + K_{ba}^{BSE}[X])Y_{ib} \end{aligned} \tag{40}$$

with e.g. the notation:

$$K_{pq}^{BSE}[X] = \sum_{jb} K_{jb,pq}^{BSE} X_{jb} \tag{41}$$

where again the (X, Y, T) are the BSE ones for a given excitation, and only the H^+ operator originates from Kohn-Sham calculations.

D. Excited-state dipole moments

We focus in the present paper on the (electronic) ES dipole moments that can be obtained as the derivative of the ES energy with respect to an external electric field. More specifically, since the BSE formalism provides the excitation energy, that is the difference of energy between a given ES and the GS, the derivative of the excitation energy Ω_λ yields the excess dipole, namely the change of the dipole from the GS to a given (λ) ES:

$$\frac{\partial \Omega_\lambda^{\mathrm{BSE}}}{\partial E_x} = \mu_{x,\lambda}^{\mathrm{ES}} - \mu_x^{\mathrm{GS}} \tag{42}$$

taking as an example an E_x field in the $\hat{x}$-direction. The transformation of the Fockian under the external electric field:

$$F_{ia} \Longrightarrow F_{ia} - eE\langle i|x|a\rangle \tag{43}$$

leads to:

$$\mu_{x,\lambda}^{\mathrm{ES}} - \mu_x^{\mathrm{GS}} = \sum_{pq} \langle p| - ex|q\rangle P_{pq} \tag{44a}$$

$$P_{pq} = T_{pq} + Z_{pq} \tag{44b}$$

where the T and Z terms originates respectively from the $\langle X,Y|\underline{G}^{(\zeta)}|X,Y\rangle$ and $\sum_{ia} Z_{ia} F_{ia}^{(\zeta)}$ terms in Eq. 23. The Z_{ij} and Z_{ab} terms, that are not calculated nor needed, are set to zero. The sum P is the relaxed difference density matrix expressed in the KS MO basis, namely the change in density matrix upon excitation.

Equation 44 clearly shows that once the Z-vector is calculated, the cost of evaluating the change of dipole along the 3 directions of space can be obtained with negligible effort. This is the simplest illustration that, in the present Lagrangian Z-vector formalism, the cost of calculating the response to several external perturbations is independent of the number of perturbations. Clearly, evaluating iteratively the Z_{ia} vector components solution of the $(A+B)Z = R$ system (see Eq. 33a) offers the same complexity as the Bethe-Salpeter eigenvalue problem to determine the (X_{ia}) excitation resonant components for e.g. the lowest S_1 excitation in the Tamm-Dancoff approximation, namely an $\mathscr{O}(N^4)$ process. As an important ingredient, and following standard strategies, we do not precalculate the left-hand-side $(A+B)$ matrix, as this would be too demanding in terms of memory. Instead, we use an iterative approach that only requires the action of the $(A+B)$ operator on test vectors in a conjugate gradient approach with the Fletcher-Reeves update scheme. This matrix$\times$vector multiplication exploits the efficient resolution-of-identity approach used at the BSE/*GW* level. An initial preconditioned Z^0-vector can be obtained as $Z_{ia}^0 = R_{ia}/(\varepsilon_a - \varepsilon_i)$ leading typically to 5-7 iterations to convergence. For sake of qualitative illustration, computing the two lowest BSE excited states of the 86 atoms push-pull $H_{42}C_{40}N_2O_2$ oligomer considered below takes about 24 mins wall-time on 256 cores (see machine characteristics in Note 79) with the cc-pVTZ basis set, while obtaining the corresponding dipole vector change from the ground-state to a given excited-state takes about 11 mins wall-time.

We conclude this Section by emphasizing that in the present BSE/ev*GW*@XCF formalism starting with a KS description of the GS, the ground-state (GS) dipole is that of the corresponding XCF functional obtained by standard DFT. As such, the ES dipole moment can be obtained by adding the DFT GS dipole to the excess dipole. Since we focus here on the BSE gradients, we will not discuss the quality of the DFT GS dipoles here. As shown in Refs. 61–64 for the systems of interest in the present study, the GS dipoles are much more stable from one formalism to another

as compared to the excess dipole. Calculating ground-state energies at the BSE level within e.g. an adiabatic-connection fluctuation–dissipation theorem (ACFDT) formalism has been explored for very small atomic or dimer systems,[43,44,80] and calculating the corresponding gradients stands well beyond the present paper.

E. Technical details

The present BSE analytic-gradients Lagrangian Z-vector formalism has been implemented in the beDeft (beyond-DFT) package, a rewriting and extension of the FIESTA code,[23,49] with an improved analytic continuation approach for the *GW* calculations,[81] the implementation of a fragment (or subsystem-based) many-body formalism,[54] and the possibility to perform cubic-scaling RPA and *GW* calculations within an accurate space-time approach.[82,83] Our many-body *GW* and BSE calculations are conducted within a Coulomb-fitting resolution-of-the-identity approach.[84–86] The BSE calculations are performed beyond the Tamm-Dancoff approximation (TDA). All occupied and virtual states are included in the construction of the Green's function, the independent-electron susceptibility used to build the screened Coulomb potential, and the BSE Hamiltonian in transition-space. All occupied and virtual states within 10 eV of the gap are explicitly corrected at the *GW* level, while lower occupied/higher virtual states are shifted rigidly following the lowest/highest explicitly corrected levels. Such a scheme ensures excellent convergence of the *GW* and BSE data. Further, *GW* calculations are performed at the partially self-consistent ev*GW* level with update of the quasiparticle energies, keeping frozen the input $\{\phi_n^{KS}\}$ one-body wavefunctions. Input HF ans KS molecular orbitals are generated with the ORCA package.[87]

We benchmark the BSE/*GW* analytical gradients on two different problems. First, we study a set of 38 transitions in 14 small molecules for which very accurate many-body wavefunction quantum chemistry ES dipoles are available.[62,63] The considered molecules and transitions are given in the SM Fig. S1. These reference calculations have been conducted at the *aug*-cc-pVTZ level to calculate GS and ES dipoles and our BSE calculations are performed at the corresponding *aug*-cc-pVTZ/*aug*-cc-pVTZ-RIFIT level. We adopt the same geometries as provided in the Supporting Information of Ref. 63 for these calculations

Second, we study the α,ω-amino,nitro-polyene oligomers containing between 1 and 20 double bonds (N). To this end, we adopt the geometries provided in Refs. 61 and 64, and perform the calculations with the cc-pVTZ/cc-pVTZ-RIFIT basis sets,[88–90] the basis set that was used to obtain

reference wavefunction data in previous studies.[61,64]

When needed, finite-field calculations are performed using a 5-point stencil formula for the derivative of a given BSE excitation energy Ω by an explicit external uniform electric field E_i (i=x, y, z):

$$\frac{\partial \Omega}{\partial E_i} = \frac{-\Omega(2\Delta E_i) + 8\Omega(\Delta E_i) - 8\Omega(-\Delta E_i) + \Omega(2\Delta E_i)}{12\Delta E_i} \tag{45}$$

with ΔE_i electric field steps of the order of 10^{-3} a.u. following numerous numerical stability tests. BSE calculations in the presence of an explicit electric field are standard BSE/evGW calculations achieved starting from KS eigenstates generated in the presence of this field. In the case of small molecules, and in particular for high-energy transitions evaluated with a diffuse-containing basis set, the proximity and crossing of numerous ES surfaces, renders the finite-field approach extremely tedious.

III. RESULTS AND DISCUSSIONS

A. Small molecules benchmark

We first explore the case of small molecules for which reference high-level wavefunction calculations exist.[62,63] This benchmark gathers 38 transitions associated with 14 molecules (see SM Fig. S1). Reference calculations, labeled below Theoretical Best Estimates (TBE), originate mainly from high-level coupled-cluster calculations up to CCSDTQ, and were performed with the *aug*-cc-pVTZ basis set. For all considered molecules, only the z-component of the excess dipole ($\Delta\mu = \mu_{z,\lambda}^{ES} - \mu_z^{GS}$) is non-zero, with a sign that corresponds to the geometries given in the Supporting Information of Ref. 63. All values calculated and used to build the upcoming figures are available in the SM (Table S2).

Let us start by providing in Fig. 1(a,b) histograms of the errors with respect to the TBE, of $\Delta\mu$ associated with standard TD-B3LYP and TD-PBE0 calculations. While TD-B3LYP and TD-PBE0 provide reasonably small errors for most transitions, with some advantage for TD-PBE0, a large number of outliers, indicated with colors, dominate the statistics. We somehow arbitrarily designate outliers states for which the TD-B3LYP error is larger than 1 Debye (D). These outliers are mostly associated with Rydberg transitions, namely the highest Σ^+ state of carbon monoxide, the B_2 state of diazirine, the B_1 state of diazomethane, the B_2 state of formaldehyde, the B_1 and A_2 states of ketene. Thioformaldehyde's $\pi \rightarrow \pi^*$ transition completes this set of challenging ES. For

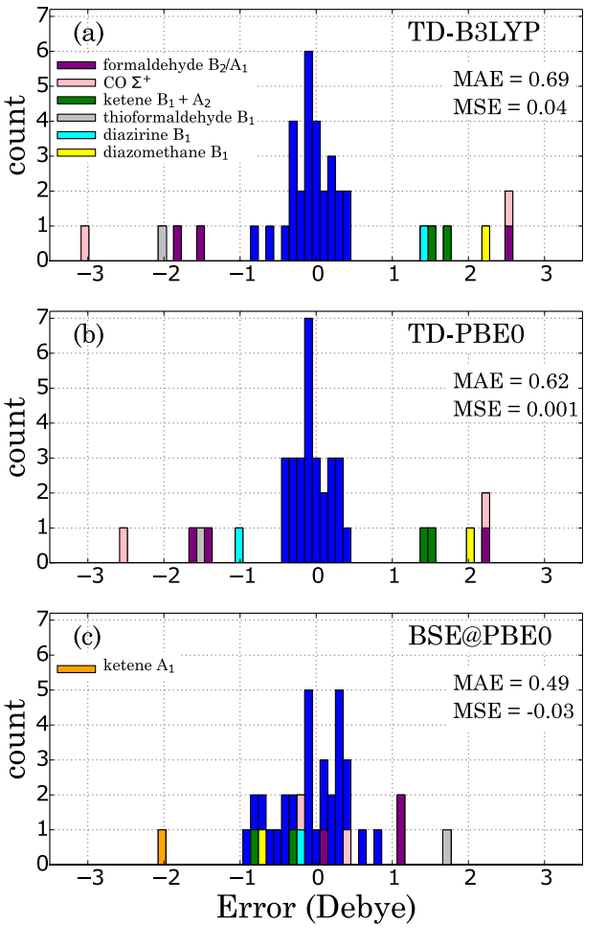

FIG. 1. Histogram for the error (Debye) associated with the excess dipole $\Delta\mu$ of 38 transitions and 14 molecules. We compare (a) TD-B3LYP, (b) TD-PBE0 and (c) the analytic BSE/ev*GW*@PBE0 to the TBE reference. Outliers are indicated with a different color code. Mean absolute (MAE) and signed (MSE) errors are indicated on the graph.

the latter case, this error of TD-B3LYP is likely due to state mixing with another close-lying state, see Ref. 63.

Rydberg excitations are characterized by diffuse final states very sensitive to the erroneous exponential tail of pure DFT exchange-correlation potentials in the vacuum, and known to be hard to describe with B3LYP.[91] This is particularly true upon using augmented basis sets allowing molecular orbitals to extend in the vacuum. Increasing the amount of exact exchange improves the situation, contributing to the expected $(-1/r)$ XCF tail stemming from exact exchange. This is evidenced by the evolution between TD-B3LYP and TD-PBE0 data with a reduction of the error associated with outliers, TD-PBE0 being known to be more suited to Rydberg ES.[92] Further, the transition from valence (localized) states to delocalized final states induces rather large

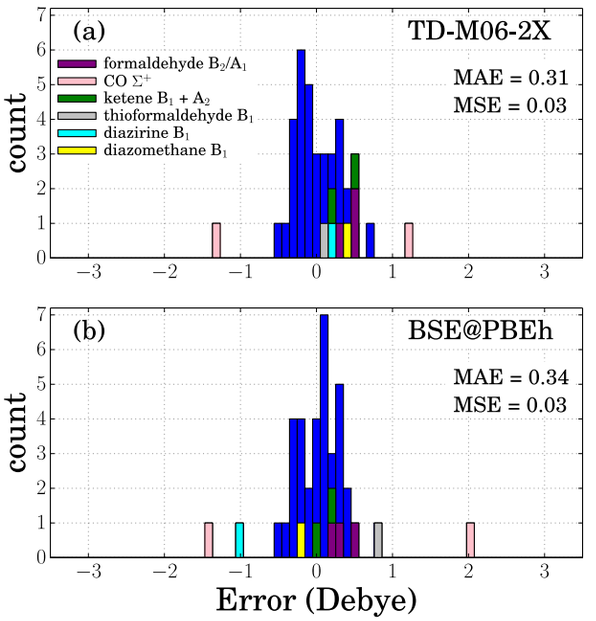

FIG. 2. Histogram for the error (Debye) as compared to TBE associated with the excess dipole $\Delta\mu$ of 38 transitions and 14 molecules. We compare in (a) TD-M06-2X with the (b) analytic BSE/ev*GW*@PBEh approach. Outliers are indicated with a different color code. The PBEh functional is the IP-tuned global hybrid optimized for each molecule (see text).

electron-hole average distance and the problem of the wrong treatment of long-range electron-hole interactions through XCF kernels with low ratio of exact exchange becomes a relevant issue.

Clearly, the analytic BSE/ev*GW*@PBE0 approach in Fig. 1(c) significantly reduces the number of outliers. We underline that within the partially self-consistent ev*GW* scheme, the shape of the delocalized orbitals inherited from DFT calculations are not corrected. However, the electron-hole interaction is correctly described by the screened Coulomb potential matrix elements, significantly contributing to alleviate the difficulties that plague TD-B3LYP and TD-PBE0 calculations. As a result the mean absolute error (MAE) obtained with BSE/ev*GW*@PBE0 is 0.49 D, smaller than its TD-B3LYP (0.69 D) and TD-PBE0 (0.62 D) counterparts.

We now compare in Fig. 2(a,b) the results of TD-M06-2X calculations with BSE/ev*GW*@PBEh(α_0), where PBEh(α_0) is the optimally tuned (OT) functional[93,94] obtained by equating the minus of the KS HOMO energy to the ΔSCF ionization potential (see data and optimal α_0 values in SM Table S2). For the present set of molecules and transitions, TD-M06-2X was shown to provide, amongst global hybrid XCF, the smallest mean absolute error, *on par* with CAM-B3LYP and ωB97X-D range-separated hybrids.[63] Concerning the BSE/ev*GW*@PBEh(α_0) approach, we rely

on the idea that OT XCF may provide KS energy gradients in best agreement with ev*GW* gradients. This is verified below.

The M06-2X functional leads to a large reduction of the number of outliers, leaving only the CO Σ^+ as problematic. As a result, the MAE is reduced to 0.31 D. A very similar result, 0.34 D, can be obtained with the BSE/ev*GW*@PBEh(α_0) data, even though, together with the same CO Σ^+ outlier, the diazirine, and to a lesser extent the thioformaldehyde B_1 Rydberg states stand out of the central $\sim[-0.5, 0.5]$ (D) main distribution. Overall, the MAE associated with the analytic ev*GW*@PBEh(α_0) approach is very close to the best TD-DFT value.

While it cannot be said that the analytic BSE gradients outperforms the best TD-DFT calculations, the large reduction of the number of outliers in both BSE/ev*GW*@PBE0 and BSE/ev*GW*@PBEh points to the much larger stability of BSE data as compared to XCF-dependent TD-DFT results. The screened Coulomb non-local kernel greatly helps in reducing the occurrence of large errors, very much independently of the starting functional. Such a conclusion was already drawn for excitation energies: BSE/ev*GW* provides good results that weakly depend on the starting XCF and on the nature of the transition (Frenkel, charge-transfer, cynanines, etc.), but does not outclass TD-DFT performed with an XCF appropriate to the state/molecule considered. The same conclusions seem to apply to the present case of ES dipole moments, a quantity much more challenging than excitation energies.

To conclude this exploration of BSE approximate analytic gradients, we compare our analytic approach to finite-field BSE/ev*GW* calculations. Our goal here is to assess the impact of the two approximations affecting the right-hand-side R_{ia} vector in the Z-vector equation scheme, namely: (a) neglecting the gradients $(\partial W/\partial\zeta)$ of the screened Coulomb potential, and (b) approximating the ev*GW*@XCF quasiparticle energy gradients by their KS XCF analogs. We emphasize at this stage that finite-field calculations are not only much more expensive than the present analytic calculations, but they are further extremely tedious in situations, often encountered when using augmented basis sets, of a large number of closely lying ES that cross under the effect of an explicit external electric field.

We first present in Fig. 3(a) the effect of freezing the screened Coulomb potential W in the BSE kernel to its zero-field expression ($W_{E=0}$) when performing our finite-field calculations. This is compared to full finite-field calculations where the screened Coulomb potential used in the BSE kernel is recalculated for each field strength value. The agreement between the two calculations is excellent, indicating that the standard practice in the BSE community to neglect the derivatives

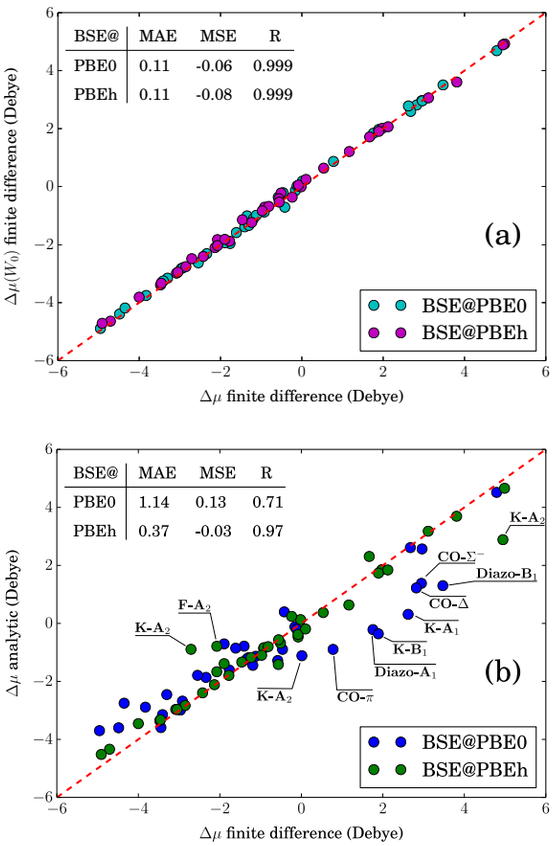

FIG. 3. Comparison of finite-field BSE/ev*GW*@XCF (XCF=PBE0, PBEh) $\Delta\mu$ excess dipoles with (a) the corresponding finite-field calculations keeping the screened Coulomb potential frozen to its zero field $W_{E=0}$ form, and (b) with the corresponding analytic calculations. The associated MAE, MSE and R values are indicated. The abbreviations K, F and Diazo stand for ketene, formaldehyde and diazomethane. The indicated CO-π outlier is the lowest lying one.

of the screened Coulomb potential is very accurate. Such results were already hinted in the exploration of *GW* quasiparticle energy ionic gradients obtained by finite-field calculations,[95] and the quality of this approximation is therefore confirmed.

We finally address the second approximation, namely replacing in R_{ia} the ev*GW*@XCF quasiparticle energy gradients by their Kohn-Sham XCF analogs. Clearly, as shown in Fig. 3(b), such an approximation is much less innocent than freezing the screened Coulomb potential, in particular when using PBE0 as starting XCF (blue dots). One notices however that the largest deviations are again associated with the most difficult cases, namely, carbon monoxide, formaldehyde, diazomethane, and ketene.

To illustrate the origin of these difficulties, we compare the evolution with respect to an applied electric field of the CO ev*GW*@XCF quasiparticle energies starting from two very different XCF, namely PBE0 and HF. As seen on Fig. 4, both the absolute energy and evolution with E-field are highly similar for most unoccupied energy levels. The same stability is observed for the occupied levels that are not shown in the Figure. However, two levels (thin lines) behave very differently with significant differences between ev*GW*@HF and ev*GW*@PBE0 data. Besides significant shifts in absolute values at zero-field, the electric-field gradients are also found to differ by about 1.5 D for these two unoccupied states.

These significant differences invalidate the central assumption common to non-self-consistent G_0W_0 or partially self-consistent ev*GW* calculations that input KS $\{\phi_n^{KS}\}$ wavefunctions are both almost equivalent with all XCF, and close to the ones that may be obtained with fully self-consistent quasiparticle qs*GW* calculations with full update of the MOs.[96] As emphasized above, this is not the case for diffuse orbitals with significant weight where the tail of the XC potential dramatically differs from one XCF to another. For such orbitals, there is in fact a sizeable inconsistency between the shape of the KS wavefunction and the tail of the *GW* self-energy away from the molecule. Such a difficulty could only be resolved by using more expensive fully self-consistent *GW* calculations or, as a pragmatic alternative, IP-tuned functionals. Along that line, molecular orbitals generated with range-separated hybrids, presenting a correct potential tail in the vacuum, may further improve the starting point as compared to the global hybrids tested here. An extensive study of the best Kohn-Sham starting point stands however beyond the present work.

In Ref. 55, the replacement of the G_0W_0@LDA quasiparticle gradients by their LDA Kohn-Sham analogs was found to be accurate for the study of the ionic gradients associated with the lowest valence Π transition of CO.[55] This is not the case for E-field gradients when using PBE0, even though the small amount of exact exchange (25%) provides a XC tail in better agreement with the correct $(-1/r)$ analytic limit than LDA. This indicates that excited-state dipole moments are much more sensitive to the presence and quality of unbound MOs than nuclear gradients. The dramatic sensitivity with basis size for these problematic ES dipole moments, as demonstrated in reference wavefunction calculations,[62,63] comes as another signature of this difficulty.

Similar conclusions apply to the other transitions affected by significant differences between analytic and finite-field BSE/ev*GW*@PBE0 data. The most dramatic case is obtained for the H_2S A_2 transition showing a difference of $\sim$ 11 D between analytic and finite-field $\Delta\mu$ values. This originates from a very large change between the (LUMO+2) PBE0 and ev*GW*@PBE0 energy level

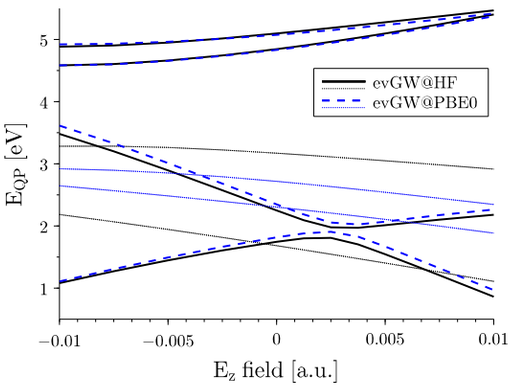

FIG. 4. Evolution with E-field of the lowest unoccupied CO ev*GW*@XCF energy levels with XCF=HF (black) and XCF=PBE0 (blue) at the *aug*-cc-pVTZ level.

E-field gradients. The analytic value is much closer (within ∼0.3 D) to the TBE reference, indicating that it is the ev*GW*@PBE0 diffuse energy level that shows a pathological behaviour under E-field. Removing the augmentation from the atomic basis reduces the error between analytic and finite-field excess dipole to ∼0.3 D showing again that indeed the problem originates from very diffuse molecular orbitals. Such a dramatic outlier has been excluded from Fig. 3(b).

The study of gradients within fully-self-consistent qs*GW* calculations stands beyond the scope of the present paper focused on the assessment of simplified analytic techniques that can compete with TD-DFT in terms of computational efficiency. We emphasize that the above-mentioned difficulties are associated with the ES dipole moments of very small systems presenting unbound diffuse unoccupied states at low energy. For such cases, we now show [Fig. 3(b) green dots] that using input Kohn-Sham orbitals generated by the IP-tuned PBEh(α_0) global hybrid dramatically improves the situation, leading to a much reduced MAE of 0.37 D, a smaller -0.05 D MSE and a large correlation coefficient (R=0.97). Outliers are reduced to the ketene and formaldehyde A_2 transitions. The difference between the analytic and finite-field H_2S A_2 $\Delta\mu$ values is reduced to below 10 mD.

B. Push-pull oligomer chains

Let us now continue our exploration of the merits of the present approximated analytic BSE gradients by considering the challenging case of increasingly long push-pull oligomers displayed

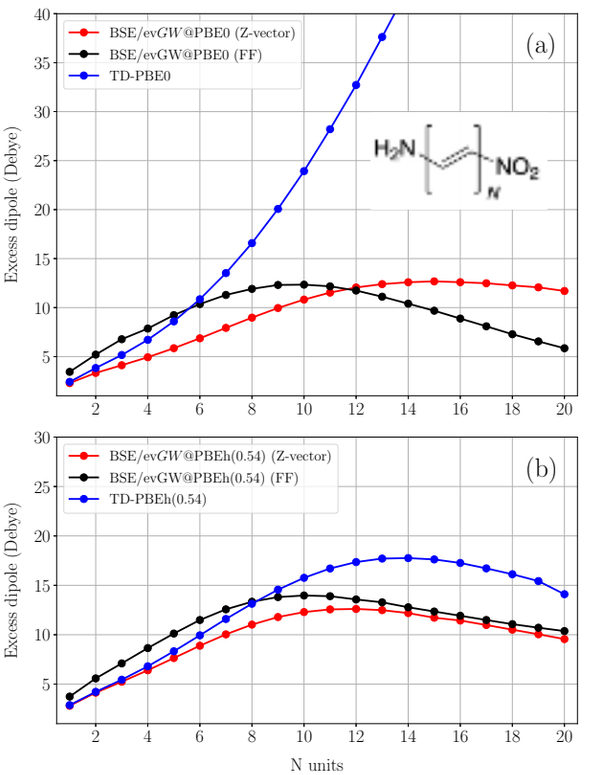

FIG. 5. Excess dipole (Debye) for the S_1 excited state of the push-pull oligomers (inset) as a function of the chain length (N). TD-XCF and finite-field (FF) BSE/evGW@XCF data are compared with the present hybrid analytic approach (Z-vector), with (a) XCF=PBE0, and (b) XCF=PBEh(0.54). Finite-field BSE calculations in (a) are from Ref. 61.

in Fig. 5(a). The excess dipole moment associated with the lowest dipole-allowed ES, that is

$$\Delta\mu = \sqrt{\sum_{i=x,y,z} (\mu_i^{\mathrm{ES}} - \mu_i^{\mathrm{GS}})^2}$$

was shown[61,64] to be characterized by dramatic changes from one theoretical approach to another, providing a stringent test case for theoretical methods. $\Delta\mu$ was already studied in a previous paper[61] at the BSE/evGW@XCF level (XCF = PBE,[97] PBE0,[98,99] CAM-B3LYP[100]) using the numerical finite-field approach only. This procedure involves a large number of ES calculations for each chain length as a function of explicit applied electric fields of various strengths, but provides reference values to which our approximated analytic approach can be compared.

Our results are presented in Fig. 5 starting by (a) a comparison of the $\Delta\mu$ as calculated within TD-PBE0 (blue dots), finite-field BSE/evGW@PBE0 (black dots) and the present analytic BSE/evGW@PBE0 (red dots) approach. The challenge of obtaining an accurate $\Delta\mu$ evolution with oligomeric length is obvious by looking at the TD-PBE0 data that present a diverging trend.

This is related to the inability for TD-DFT calculations, with XCF presenting a too small percentage of exact exchange, to properly account for long-range electron-hole interactions.[101,102] As shown in Ref. 61 by comparison with wavefunction approaches [ADC(2), CC2, and CCSD] and as reproduced in Fig. 5(a), the proper behavior is restored by the finite-field BSE/evGW@PBE0 calculations (black dots): $\Delta\mu$ starts increasing with length before reaching a plateau and decaying for long chains. The value of the maximum $\Delta\mu$ was shown to vary from $\sim$23 D at the CC2 level to $\sim$18 D at the less approximated CCSD level. BSE/evGW@XCF calculations yield a stable value of $\sim$12 D with XCF=PBE, PBE0, and CAM-B3LYP.[61] These rather large variations from one approach to another confirm the challenging nature of this problem. However, both BSE and wavefunction methods deliver the very same behavior.

The Z-vector analytic approach to BSE/evGW@PBE0 gradients [Fig. 5(a) red dots; data in the SM Table S3] provides the correct behavior, a dramatic improvement as compared to TD-PBE0. This stems from the replacement of the PBE0 kernel by the non-local screened Coulomb potential that enforces physically-correct long-range electron-hole attractive interaction. Nevertheless, the two approximations performed on the R_{ia} term, namely freezing the screened Coulomb potential to its zero-field value, and replacing the evGW@PBE0 quasiparticle energy gradients by their PBE0 KS analogs, clearly induce some deviations with respect to the reference finite-field BSE calculations. For the longest chains, the analytic scheme present features of both TD-PBE0 and BSE approaches, with a slower decay of the excess dipole as a likely inheritance of the TD-PBE0 divergence. As discussed above, it is mainly the second approximation that is responsible for the difference between the analytic and the finite-field BSE results.

Fig. 5(b) considers as a starting XCF the PBEh(0.54), a global hybrid containing 54% of exact exchange, similar to what is used in M06-2X.[103] This admixture represents some averaged value of optimally-tuned (OT) exact exchange ratio obtained by tuning the XCF such that the negative of the KS HOMO energy equals the ΔSCF ionisation potential. In fact, the OT amount of exact exchange ranges from $\alpha = 59\%$ for N=8, before the maximum $\Delta\mu$ value, to $\alpha = 52\%$ for the longest N=20 chain, *i.e.*, the 54% XCF is a reasonable and simple choice for all chain lengths. The use of an IP-tuned functional is consistent with the present approach and the assumption that KS gradients obtained with an OT functional may be closer to evGW gradients, as already hinted in the study of small molecules. The improved agreement between the approximate analytic approach and the finite-field reference data is another indication of the validity of this assumption. The TD-PBEh(0.54) and BSE/evGW@PBEh(0.54) results are compiled in the SM Table S4.

We conclude this Section by observing that the analytic BSE approach allows curing the pathological behavior associated with TD-PBE0, or any TD-DFT calculation relying on an XCF with a low exact exchange ratio, with a formalism offering the same cost as modern Z-vector implementations of TD-DFT analytic gradients. Further, the maximum $\Delta\mu$ is stable, ca. 12.6-12.7 D, starting with the very different PBE0 and PBEh(0.54) XCF, with a position for this maximum that evolves from N=12 to N=15. The larger variations in maximum value between ADC(2), CC2 and CCSD calculations,[61,64] notwithstanding the dramatic differences between various TD-DFT calculations, indicate that the analytic BSE/evGW@XCF scheme ensures not only the correct behavior, but also offers a significant stability of the results as a function of the starting XCF, despite the replacement of the quasiparticle energy gradients by their Kohn-Sham analogs.

IV. CONCLUSIONS

We have implemented and explored the *pros* and *cons* of a simple approach to Bethe-Salpeter analytic gradients within a Lagrangian Z-vector formalism, taking, as a first application, the ES dipole moments associated with the gradient of the ES energy with respect to an electric field. Such an approach, similar to modern techniques implemented in TD-DFT codes, allows determining the gradients with respect to several perturbations for a cost equivalent to a single BSE calculation on the unperturbed system. Our approach has been benchmarked considering on the one hand a family of very small molecules for which reference quantum chemistry data are available, and on the other hand the challenging case of increasingly long push-pull oligomers.

The simplicity of the present approach relies on two approximations already advocated in a pioneering study of the BSE nuclear gradients in CO and NH_3.[55] In the present formulation, such approximations affect only the R_{ia} right-hand-side term of the Z-vector equation. Indeed, when BSE/GW calculation rely on standard non-self-consistent G_0W_0 or partially self-consistent evGW techniques, keeping the input Kohn-Sham eigenstates frozen, the left hand-side $(A+B)$ matrix acting on the Z-vector is found to be rigorously the same as in the corresponding TD-DFT problem where the same exchange-correlation functional is used.

The first simplification to the R_{ia} term is the neglect of the screened Coulomb potential gradients $(\partial W/\partial\zeta)$. Such an approximation is found to be very accurate, dramatically simplifying the implementation of the BSE analytic gradients. The second approximation is the replacement of the quasiparticle energy gradients by their KS analogs. This latter simplification generally leads to

quantitative differences between the approximated BSE analytic gradients and those obtained by finite difference. Such differences are however significantly reduced upon adopting an IP-tuned XCF as a starting point for BSE/*GW* calculations.

Independently of the deviations between the approximate analytic and exact BSE gradients obtained by finite differences, the use of the approximate BSE analytic gradients dramatically reduces the number of pathological cases encountered with TD-DFT when using standard global hybrids such as B3LYP or PBE0, providing results that compare well with those obtained with the "best" TD-DFT calculations, a statement especially true for Rydberg transitions. This is a significant advantage of the BSE approach, already noticed for the calculation of vertical excitation energies, that the impact of the starting XCF functional is dramatically reduced, providing reliable results for local (Frenkel), charge-transfer, cyanine, Rydberg, etc. transitions for which TD-DFT might fail, or at least, require various XCF to deliver reasonable results.

In the light of the encouraging present results, the impact of the second approximation, consisting in adopting Kohn-Sham energy level gradients in the right-hand-side R_{ia} term, could be bypassed in the future by calculating *GW* energy level gradients. The derivatives of the independent electron susceptibility has been worked out in the context of the RPA ground-state forces,[104] paving the way to calculating the screened Coulomb potential gradients. However, the accuracy of the approximation consisting in neglecting the W-gradients advocates a pragmatic approach where only the Green's function G in the *GW* self-energy needs to be differentiated. The possibility to derive G efficiently at constant molecular orbitals $\{C_{n\mu}\}$ coefficients in a framework consistent with the Lagrangian approach is currently under study. The use of such approximate *GW* quasiparticle gradients may further reduce, at a reasonable cost, the impact of the choice of the input DFT XCF.

Finally, the implementation of ionic gradients, and the verification on large molecular sets that this second approximation is in that case more accurate than for excited-state dipole moments, stands as a forthcoming extension of the present study. Following the arguments detailed above, the Z-vector equation remains the same since independent of the applied perturbation. Further, the derivatives $F^{(\zeta)}$ and $S^{(\zeta)}$ at constant $\{C_{n\mu}\}$ with respect to ionic degrees of freedom of the one-body Hamiltonian and overlap matrix are the same as the one used in TD-DFT,[8] and only the $G^{(\zeta)}$ constrained derivative changes from its TD-DFT to its BSE expression. Here again, the constant-W approximation is expected to be very accurate.

SUPPLEMENTARY MATERIAL

See the Supplementary Material for the validation at the TD-HF level of our *Z*-vector implementation, a description of the small molecules and transitions involved in our benchmark, and all data associated with the small molecules and long chains.

ACKNOWLEDGMENTS

The project received support from the French Agence Nationale de la Recherche (ANR) under contract ANR-20-CE29-0005 (BSE-Forces). This work used computational resources generously provided by the CCIPL computational center installed in Nantes and the national HPC facilities under contract GENCI-TGCC A0110910016.

DATA AVAILABILITY STATEMENT

AVAILABILITY OF DATA	STATEMENT OF DATA AVAILABILITY
Data available in article or supplementary material	The data that support the findings of this study are available within the article [and its supplementary material].

REFERENCES

[1]J. Lombardi, Spectrochim. Acta A **43**, 1323 (1987).

[2]M. Schmitt and L. Meerts, *Frontiers and Advances in Molecular Spectroscopy*, edited by J. Laane (Elsevier, 2018).

[3]J. Gerratt and I. M. Mills, J. Chem. Phys. **49**, 1719 (1968), https://doi.org/10.1063/1.1670299.

[4]J. A. Pople, R. Krishnan, H. B. Schlegel, and J. S. Binkley, Int. J. Quant. Chem. **16**, 225 (1979), https://onlinelibrary.wiley.com/doi/pdf/10.1002/qua.560160825.

[5]M. Frisch, M. Head-Gordon, and J. Pople, Chem. Phys. **141**, 189 (1990).

[6]N. C. Handy and H. F. Schaefer, J. Chem. Phys. **81**, 5031 (1984).

[7]T. Helgaker and P. Jorgensen, Theor. Chim. Acta **75**, 111 (1989).

[8]F. Furche and R. Ahlrichs, J. Chem. Phys. **117**, 7433 (2002), https://doi.org/10.1063/1.1508368.

[9]C. Van Caillie and R. D. Amos, Chem. Phys. Lett. **308**, 249 (1999).

[10]G. Scalmani, M. J. Frisch, B. Mennucci, J. Tomasi, R. Cammi, and V. Barone, J. Chem. Phys. **124**, 094107 (2006), https://doi.org/10.1063/1.2173258.

[11]A. Kovyrshin and J. Neugebauer, Phys. Chem. Chem. Phys. **18**, 20955 (2016).

[12]T. Helgaker, P. Jørgensen, and N. Handy, Theoret. Chim. Acta (1989).

[13]A. Köhn and C. Hättig, J. Chem. Phys. **119**, 5021 (2003), https://doi.org/10.1063/1.1597635.

[14]M. Kállay and J. Gauss, J. Chem. Phys. **121**, 9257 (2004), https://doi.org/10.1063/1.1805494.

[15]G. Csanak, H. Taylor, and R. Yaris (Academic Press, 1971) pp. 287–361.

[16]W. Hanke and L. J. Sham, Phys. Rev. Lett. **43**, 387 (1979).

[17]G. Strinati, Riv. del Nuovo Cim. **11**, 1 (1988).

[18]S. Albrecht, L. Reining, R. Del Sole, and G. Onida, Phys. Rev. Lett. **80**, 4510 (1998).

[19]M. Rohlfing and S. G. Louie, Phys. Rev. Lett. **81**, 2312 (1998).

[20]E. L. Shirley, Phys. Rev. Lett. **80**, 794 (1998).

[21]D. Jacquemin, I. Duchemin, and X. Blase, J. Chem. Theory Comput. **11**, 3290 (2015), pMID: 26207104, https://doi.org/10.1021/acs.jctc.5b00304.

[22]F. Bruneval, S. M. Hamed, and J. B. Neaton, J. Chem. Phys. **142**, 244101 (2015), https://doi.org/10.1063/1.4922489.

[23]D. Jacquemin, I. Duchemin, and X. Blase, J. Phys. Chem. Lett. **8**, 1524 (2017), pMID: 28301726, https://doi.org/10.1021/acs.jpclett.7b00381.

[24]X. Gui, C. Holzer, and W. Klopper, J. Chem. Theory Comput. **14**, 2127 (2018), pMID: 29499116, https://doi.org/10.1021/acs.jctc.8b00014.

[25]V. Ziaei and T. Bredow, J. Phys.: Cond. Matt. **30**, 395501 (2018).

[26]J. D. Elliott, N. Colonna, M. Marsili, N. Marzari, and P. Umari, J. Chem. Theory Comput. **15**, 3710 (2019), pMID: 30998361, https://doi.org/10.1021/acs.jctc.8b01271.

[27]N. L. Nguyen, H. Ma, M. Govoni, F. Gygi, and G. Galli, Phys. Rev. Lett. **122**, 237402 (2019).

[28]C. Liu, J. Kloppenburg, Y. Yao, X. Ren, H. Appel, Y. Kanai, and V. Blum, J. Chem. Phys. **152**, 044105 (2020), https://doi.org/10.1063/1.5123290.

[29]K. Hummer, P. Puschnig, and C. Ambrosch-Draxl, Phys. Rev. Lett. **92**, 147402 (2004).

[30]X. Blase and C. Attaccalite, Appl. Phys. Lett. **99**, 171909 (2011), https://doi.org/10.1063/1.3655352.

[31]B. Baumeier, D. Andrienko, and M. Rohlfing, J. Chem. Theory Comput. **8**, 2790 (2012), pMID: 26592120, https://doi.org/10.1021/ct300311x.

[32]I. Duchemin, T. Deutsch, and X. Blase, Phys. Rev. Lett. **109**, 167801 (2012).

[33]P. Cudazzo, M. Gatti, A. Rubio, and F. Sottile, Phys. Rev. B **88**, 195152 (2013).

[34]S. Sharifzadeh, P. Darancet, L. Kronik, and J. B. Neaton, J. Phys. Chem. Lett. **4**, 2197 (2013), https://doi.org/10.1021/jz401069f.

[35]V. Ziaei and T. Bredow, J. Chem. Phys. **145**, 174305 (2016), https://doi.org/10.1063/1.4966920.

[36]P. Boulanger, D. Jacquemin, I. Duchemin, and X. Blase, J. Chem. Theory Comput. **10**, 1212 (2014), pMID: 26580191, https://doi.org/10.1021/ct401101u.

[37]Y. Ma, M. Rohlfing, and C. Molteni, Phys. Rev. B **80**, 241405 (2009).

[38]D. Zhang, S. N. Steinmann, and W. Yang, J. Chem. Phys. **139**, 154109 (2013), https://doi.org/10.1063/1.4824907.

[39]V. Olevano, J. Toulouse, and P. Schuck, J. Chem. Phys. **150**, 084112 (2019), https://doi.org/10.1063/1.5080330.

[40]P.-F. Loos and X. Blase, J. Chem. Phys. **153**, 114120 (2020), https://doi.org/10.1063/5.0023168.

[41]S. J. Bintrim and T. C. Berkelbach, J. Chem. Phys. **156**, 044114 (2022), https://doi.org/10.1063/5.0074434.

[42]T. Olsen and K. S. Thygesen, J. Chem. Phys. **140**, 164116 (2014), https://doi.org/10.1063/1.4871875.

[43]C. Holzer, X. Gui, M. E. Harding, G. Kresse, T. Helgaker, and W. Klopper, J. Chem. Phys. **149**, 144106 (2018), https://doi.org/10.1063/1.5047030.

[44]P.-F. Loos, A. Scemama, I. Duchemin, D. Jacquemin, and X. Blase, J. Phys. Chem. Lett. **11**, 3536 (2020), pMID: 32298578, https://doi.org/10.1021/acs.jpclett.0c00460.

[45]W. Olovsson, I. Tanaka, T. Mizoguchi, P. Puschnig, and C. Ambrosch-Draxl, Phys. Rev. B **79**, 041102 (2009).

[46]J. Vinson, J. J. Rehr, J. J. Kas, and E. L. Shirley, Phys. Rev. B **83**, 115106 (2011).

[47]Y. Yao, D. Golze, P. Rinke, V. Blum, and Y. Kanai, J. Chem. Theory Comput. **18**, 1569 (2022), pMID: 35138865, https://doi.org/10.1021/acs.jctc.1c01180.

[48]I. Duchemin, D. Jacquemin, and X. Blase, J. Chem. Phys. **144**, 164106 (2016), https://doi.org/10.1063/1.4946778.

[49]I. Duchemin, C. A. Guido, D. Jacquemin, and X. Blase, Chem. Sci. **9**, 4430 (2018).

[50]B. Baumeier, M. Rohlfing, and D. Andrienko, J. Chem. Theory Comput. **10**, 3104 (2014), pMID: 26588281, https://doi.org/10.1021/ct500479f.

[51]J. Li, G. D'Avino, I. Duchemin, D. Beljonne, and X. Blase, J. Phys. Chem. Lett. **7**, 2814 (2016), pMID: 27388926, https://doi.org/10.1021/acs.jpclett.6b01302.

[52]J. Tölle, T. Deilmann, M. Rohlfing, and J. Neugebauer, J. Chem. Theory Comput. **17**, 2186 (2021), pMID: 33683119, https://doi.org/10.1021/acs.jctc.0c01307.

[53]T. Fujita and Y. Noguchi, J. Phys. Chem. A **125**, 10580 (2021), pMID: 34871000, https://doi.org/10.1021/acs.jpca.1c07337.

[54]D. Amblard, G. D'Avino, I. Duchemin, and X. Blase, Phys. Rev. Materials **6**, 064008 (2022).

[55]S. Ismail-Beigi and S. G. Louie, Phys. Rev. Lett. **90**, 076401 (2003).

[56]X. Gonze, D. C. Allan, and M. P. Teter, Phys. Rev. Lett. **68**, 3603 (1992).

[57]O. Çaylak and B. Baumeier, J. Chem. Theory Comput. **17**, 879 (2021), pMID: 33399447, https://doi.org/10.1021/acs.jctc.0c01099.

[58]M. S. Kaczmarski, Y. Ma, and M. Rohlfing, Phys. Rev. B **81**, 115433 (2010).

[59]I. Knysh, I. Duchemin, X. Blase, and D. M. Jacquemin, J. Chem. Phys. **0**, null (0), https://doi.org/10.1063/5.0121121.

[60]I. Knysh, K. Letellier, I. Duchemin, X. Blase, and D. Jacquemin, Phys. Chem. Chem. Phys. **25**, 8376 (2023).

[61]I. Knysh, J. D. J. Villalobos-Castro, I. Duchemin, X. Blase, and D. Jacquemin, J. Phys. Chem. Lett. **14**, 3727 (2023), pMID: 37042642, https://doi.org/10.1021/acs.jpclett.3c00699.

[62]A. Chrayteh, A. Blondel, P.-F. Loos, and D. Jacquemin, J. Chem. Theory Comput. **17**, 416 (2021), pMID: 33256412, https://doi.org/10.1021/acs.jctc.0c01111.

[63]R. Sarkar, M. Boggio-Pasqua, P.-F. Loos, and D. Jacquemin, J. Chem. Theory Comput. **17**, 1117 (2021), pMID: 33492950, https://doi.org/10.1021/acs.jctc.0c01228.

[64]D. Jacquemin, J. Chem. Theory Comput. **12**, 3993 (2016), pMID: 27385324, https://doi.org/10.1021/acs.jctc.6b00498.

[65]L. Hedin, Phys. Rev. **139**, A796 (1965).

[66]G. Strinati, H. J. Mattausch, and W. Hanke, Phys. Rev. Lett. **45**, 290 (1980).

[67]M. S. Hybertsen and S. G. Louie, Phys. Rev. B **34**, 5390 (1986).

[68]R. W. Godby, M. Schlüter, and L. J. Sham, Phys. Rev. B **37**, 10159 (1988).

[69]F. Aryasetiawan and O. Gunnarsson, Rep. Prog. Phys. **61**, 237 (1998).

[70]B. Farid, *Electron Correlation in the Solid State - Chapter 3*, edited by N. March (Imperial College Press, London, 1999).

[71]G. Onida, L. Reining, and A. Rubio, Rev. Mod. Phys. **74**, 601 (2002).

[72]Y. Ping, D. Rocca, and G. Galli, Chem. Soc. Rev. **42**, 2437 (2013).

[73]D. Golze, M. Dvorak, and P. Rinke, Front. Chem. **7**, 377 (2019).

[74]R. Martin, L. Reining, and D. Ceperley, *Interacting Electrons: Theory and Computational Approaches* (Cambridge University Press, 2016).

[75]X. Blase, I. Duchemin, D. Jacquemin, and P.-F. Loos, J. Phys. Chem. Lett. **11**, 7371 (2020), pMID: 32787315, https://doi.org/10.1021/acs.jpclett.0c01875.

[76]F. Kaplan, M. E. Harding, C. Seiler, F. Weigend, F. Evers, and M. J. van Setten, J. Chem. Theory Comput. **12**, 2528 (2016), pMID: 27168352, https://doi.org/10.1021/acs.jctc.5b01238.

[77]X. Gonze, Phys. Rev. A **52**, 1096 (1995).

[78]S. Baroni, S. de Gironcoli, A. Dal Corso, and P. Giannozzi, Rev. Mod. Phys. **73**, 515 (2001).

[79]Calculations performed on the French Irene Rome supercomputer with 2.6 GHz AMD Rome (Epyc) cores and 2 Gb/core memory.

[80]J. Li, N. D. Drummond, P. Schuck, and V. Olevano, SciPost Phys. **6**, 040 (2019).

[81]I. Duchemin and X. Blase, J. Chem. Theory Comput. **16**, 1742 (2020).

[82]I. Duchemin and X. Blase, J. Chem. Phys. **150**, 174120 (2019), https://doi.org/10.1063/1.5090605.

[83]I. Duchemin and X. Blase, J. Chem. Theory Comput. **17**, 2383 (2021), pMID: 33797245, https://doi.org/10.1021/acs.jctc.1c00101.

[84]J. L. Whitten, J. Chem. Phys. **58**, 4496 (1973), https://doi.org/10.1063/1.1679012.

[85]X. Ren, P. Rinke, V. Blum, J. Wieferink, A. Tkatchenko, A. Sanfilippo, K. Reuter, and M. Scheffler, New J. Phys. **14**, 053020 (2012).

[86]I. Duchemin, J. Li, and X. Blase, J. Chem. Theory Comput. **13**, 1199 (2017), pMID: 28094983, https://doi.org/10.1021/acs.jctc.6b01215.

[87]F. Neese, WIREs Comput. Mol. Sci. **2**, 73 (2012).

[88]F. Weigend, A. Köhn, and C. Hättig, J. Chem. Phys. **116**, 3175 (2002).

[89]T. H. Dunning, J. Chem. Phys. **90**, 1007 (1989), https://doi.org/10.1063/1.456153.

[90]R. A. Kendall, T. H. Dunning, and R. J. Harrison, J. Chem. Phys. **96**, 6796 (1992), https://doi.org/10.1063/1.462569.

[91]M. J. G. Peach, P. Benfield, T. Helgaker, and D. J. Tozer, J. Chem. Phys. **128**, 044118 (2008).

[92]I. Ciofini and C. Adamo, J. Phys. Chem. A **111**, 5549 (2007), https://doi.org/10.1021/jp0722152.

[93]R. Baer, E. Livshits, and U. Salzner, Ann. Rev. Phys. Chem. **61**, 85 (2010).

[94]L. Kronik, T. Stein, S. Refaely-Ambrason, and R. Baer, J. Chem. Theory Comput. **8**, 1515 (2012).

[95]C. Faber, P. Boulanger, C. Attaccalite, E. Cannuccia, I. Duchemin, T. Deutsch, and X. Blase, Phys. Rev. B **91**, 155109 (2015).

[96]M. van Schilfgaarde, T. Kotani, and S. Faleev, Phys. Rev. Lett. **96**, 226402 (2006).

[97]J. P. Perdew, K. Burke, and M. Ernzerhof, Phys. Rev. Lett. **77**, 3865 (1996).

[98]J. P. Perdew, M. Ernzerhof, and K. Burke, J. Chem. Phys. **105**, 9982 (1996), https://doi.org/10.1063/1.472933.

[99]C. Adamo and V. Barone, J. Chem. Phys. **110**, 6158 (1999), https://doi.org/10.1063/1.478522.

[100]Chem. Phys. Lett. **393**, 51 (2004).

[101]A. Dreuw and M. Head-Gordon, J. Am. Chem. Soc. **126**, 4007 (2004), pMID: 15038755, https://doi.org/10.1021/ja039556n.

[102]S. Botti, F. Sottile, N. Vast, V. Olevano, L. Reining, H.-C. Weissker, A. Rubio, G. Onida, R. Del Sole, and R. W. Godby, Phys. Rev. B **69**, 155112 (2004).

[103]Y. Zhao, N. E. Schultz, and D. G. Truhlar, J. Chem. Theory Comput. **2**, 364 (2006), pMID: 26626525, https://doi.org/10.1021/ct0502763.

[104]B. Ramberger, T. Schäfer, and G. Kresse, Phys. Rev. Lett. **118**, 106403 (2017).